IEEE Access
Multidisciplinary : Rapid Review : Open Access Journal
IEEE POWER & ENERGY SOCIETY SECTION

Received October 2, 2019, accepted October 22, 2019, date of publication November 6, 2019, date of current version November 15, 2019.

Digital Object Identifier 10.1109/ACCESS.2019.2951748

A Hardware-In-the-Loop Test on the Multi-Objective Ancillary Service by In-Vehicle Batteries: Primary Frequency Control and Distribution Voltage Support

NAOTO MIZUTA[1], SHOTARO KAMO[2], HIDEKUNI TODA[2], YOSHIHIKO SUSUKI[1], (Member, IEEE), YUTAKA OTA[2], (Member, IEEE), AND ATSUSHI ISHIGAME[1], (Member, IEEE)

[1]Department of Electrical and Information Systems, Osaka Prefecture University, Sakai 599-8531, Japan
[2]Department of Electrical and Electronics Engineering, Tokyo City University, Tokyo 158-8557, Japan

Corresponding author: Yoshihiko Susuki (susuki@eis.osakafu-u.ac.jp)

This work was supported by the Japan Science and Technology Agency (JST), Core Research for Evolutional Science and Technology (CREST) Program Grant Number JP-MJCR15K3, Japan.

ABSTRACT The motivation of our research is to pursue a possibility of utilizing electric vehicles for the future operation of power transmission and distribution grids. In this paper, we report a Power-Hardware-In-the-Loop (Power-HIL) testing on the provision of Ancillary Service (AS) by in-vehicle batteries. The AS of our interest is multi-objective in the sense that it simultaneously provides both primary frequency control reserve for a transmission grid and voltage support for a high-voltage distribution grid. The Power-HIL testing is crucial to validating the Multi-Objective AS because the dynamics of the grids and of power conditioning systems emerge in a common time scale, latter of which involves modeling difficulties and thus needs their inclusion as real physical devices, that is, Power-HIL. We show that the Multi-Objective AS is simulated consistently in a Power-HIL testbed and works effectively in a dynamic situation of transmission and distribution grids.

INDEX TERMS Ancillary service, electric vehicle, frequency control, hardware-in-the-loop, power system, vehicle-to-grid, voltage control.

I. INTRODUCTION

The utilization of Electric Vehicles (EVs) is a promising technology in the future operation of power transmission and distribution grids. The so-called Demand Response (DR) in a transmission grid aims to shift the peak load and to provide regulation supports for primary and secondary (load) frequency control, where a large population of in-vehicle batteries are utilized in a coordinated manner: see, e.g., [1], [2]. The so-called *Distribution System Operator* (DSO) (see, e.g., [3]) is investigated for managing such batteries in order to conduct the DR as a load dispatching center or aggregator. The system-level coordinations are generally termed as *Ancillary Service* (AS) [4] provided by EVs and have been attracting a lot of interest in research and development since 2005: see, e.g., [5]–[8].

The associate editor coordinating the review of this manuscript and approving it for publication was Ravindra Singh.

TABLE 1. List of abbreviation used in this paper.

AS:	Ancillary Service
DR:	Demand Response
DSO:	Distribution System Operator
EDC:	Economic Dispatch Control
EV:	Electric Vehicle
HIL:	Hardware-In-the-Loop
ODE:	Ordinary Differential Equation
PCS:	Power Conditioning System
PFC:	Primary Frequency Control
PV:	Photo-Voltaic

The provision of AS by EVs poses several problems on the distribution grid. One major problem is to manage the impact of charging/discharging of a large population of EVs to the distribution voltage. An EV is regarded as an autonomously moving battery in the spatial domain and can conduct the charging and discharging everywhere in the grid. Thus, maintaining the nominal distribution voltage while providing the AS by EVs is a challenging subject. In fact, Clement-Nyns *et al.* [9], [10] study the impact of EV charging to the distribution grid using the load-flow analysis and propose optimization-based methods for determining the timing and amount of charging power in order to reduce the voltage deviation. Also, the provision of voltage control supports by EVs has been studied: see, e.g., [11], [12].

In [13], [14], we developed a simple algorithm to synthesize a spatial pattern of charging/discharging operations of in-vehicle batteries for providing the Primary Frequency Control (PFC) reserve as well as mitigating its voltage impact, to which we refer as the *Multi-Objective AS*. PFC is called frequency response in PJM [4] and needs the fast responsiveness in AS that is of several hundred milliseconds to several seconds [15]. This algorithm is based on the so-called nonlinear ODE (Ordinary Differential Equation) representation of distribution voltage [16]. A situation for the algorithm is intended in [14], where a DSO works as a provider of the PFC reserve by coordinated use of EVs and receives a regulation signal from a transmission system operator, termed as the PFC signal. The algorithm makes it possible for the DSO to determine the values of charging/discharging power (active and reactive) by in-vehicle batteries in a distribution grid, so that active power corresponding to the PFC signal is provided, and the deviation of distribution voltage from a nominal value is reduced: see Section II in detail.

The purpose of this paper is to report a laboratory testing on the Multi-Objective AS by in-vehicle batteries. We do this testing with a *Hardware-In-the-Loop* (HIL) testbed. HIL or Power-HIL is an efficient method for real-time testing of the coupling between digital simulators and real electrical devices in the power technology [17]. The Multi-Objective AS is intended to regulate the dynamics of the grid's frequency—in order of several seconds—by inverter-interfaced batteries on a distribution grid. Therefore, the AS signal allocated to each battery changes temporally in the same time scale of the frequency dynamics and works as an external forcing to the grid. The time scale is included in that of dynamic characteristics of power conversion by inverters or Power Conditioning Systems (PCSs) (see Section IV) that involve modeling difficulties as stated by many researchers, e.g., [18]. This clearly needs their inclusion as real physical devices for simulation studies on the AS provision, namely, the Power-HIL testing.

The importance of HIL for validating the AS provision of power-electronics-interfaced distributed generations is discussed in [18]. The authors of [15] use series-produced EVs for experimental validation for PFC in a laboratory environment. In [19], the power quality issue in low-voltage networks, i.e. voltage quality is addressed in the same laboratory environment. Also, the authors of [20] report a field test validation of the AS provision of several types including PFC and local voltage support.

The content and contributions of this paper are summarized below. A Power-HIL testbed is developed in [21], [22] for experimental studies on the frequency control of a transmission grid by smart inverters and on the voltage management of a distribution grid. In this paper, based on [13], [14], [21], [22], we report a series of experimental data of the Power-HIL testing on the Multi-Objective AS by in-vehicle batteries for a simple setup of transmission and distribution grids. The main contributions of this paper are twofold. First, using the Power-HIL testbed, we show that the dynamics of frequency and voltage under the Multi-Objective AS are *consistently simulated*. This simulation is done in a connection of multiple components occurring in practice such as hardware, software (digital simulator), communication lines, and measurement devices. Second, we show that the Multi-Objective AS, technically, the algorithm in [13], [14] works in a *dynamic* situation, where both the grid's frequency and distribution voltage profile can change in time. Validating its effectiveness in the dynamic situation is novel. It is noted that there is no prior publication on the work presented in this paper.

The rest of this paper is organized as follows: in Section II we review the algorithm for synthesis of charging/discharging operation of in-vehicle batteries proposed in [13], [14]. In Section III we introduce the Power-HIL testbed that we use throughout this paper. In Section IV we report a series of experimental data on the Power-HIL testing and validate its performance. Section V is the conclusion of this paper with a summary and future work.

II. MULTI-OBJECTIVE ANCILLARY SERVICE BY IN-VEHICLE BATTERIES

In this section, we review the algorithm for provision of the Multi-Objective AS—PFC and distribution voltage support—based on [13], [14].

A. ODE REPRESENTATION OF DISTRIBUTION VOLTAGE

The algorithm validated in this paper is based on the ODE representation of distribution voltage profile, which was developed in [16]. For simplicity of its introduction, we assume that no voltage regulation device such as load ratio control transformer and step voltage regulator is operated. Thus, we can consider the voltage profile starting at a distribution substation (bank) that is continuous in space (length). It is shown in [23] that the effect of such regulation devices can be included in the ODE representation. Now, consider a single, straight-line distribution feeder shown in Figure 1, starting at a bank where we introduce the origin of one-dimensional displacement (location) $x \in \mathbb{R}$ as $x = 0$. The voltage phasor at the location x is represented with $v(x)\exp\{\sqrt{-1}\theta(x)\}$, where $v(x)$ stands for the *voltage amplitude* [V] and $\theta(x)$ for the *voltage phase* [rad]. Also, as new functions in x, define the *power transfer density* [V^2/km] at x by $s(x) := -v(x)^2 d\theta(x)/dx$ and the *voltage gradient* [V/km] by $w(x) := dv(x)/dx$. Then, the four unknown functions v, θ, s, and w are related in the

FIGURE 1. A single, straight-line distribution feeder that starts at a bank, through a finite-length line with length *L*, and ends at a non-loading terminal.

following nonlinear ODE [16]:

$$\left.\begin{aligned} \frac{dv}{dx} &= w, \\ \frac{d\theta}{dx} &= -\frac{s}{v^2} \quad (v \neq 0), \\ \frac{ds}{dx} &= \frac{Bp(x) - Gq(x)}{G^2 + B^2}, \\ \frac{dw}{dx} &= \frac{s^2}{v^3} - \frac{Gp(x) + Bq(x)}{v(G^2 + B^2)}. \end{aligned}\right\} \tag{1}$$

The constants G and B are the conductance and susceptance per unit-length [S/km]. Also, the function $p(x)$ (or $q(x)$) is the active (or reactive) power flowing into the feeder (note that $p(x) > 0$ indicates the positive active-power flowing to the feeder at x). We will call $p(x)$ and $q(x)$ the *power density functions* [W/km] and [Var/km], respectively.

Here, based on (1), we introduce an approximate representation of the voltage gradient $w(x)$ that is a basis of the synthesis algorithm. To this end, consider a case where multiple charging stations as well as pure resistive loads are connected to the feeder in Figure 1. We suppose that N number of stations and loads are located at $x = \xi_i \in (0, L)$ $(i = 1, \dots, N)$ satisfying $\xi_{i+1} < \xi_i$, and that in-vehicle batteries and loads are operated under unity-power factor. This implies $q(x) = 0$ for all x and is relevant in the current practice of vehicle-to-grid.[1] By denoting as P_i the active-power discharged ($P_i > 0$) or charged (consumed; $P_i < 0$) at $x = \xi_i$, the power density function $p(x)$ is given as $p(x) = \sum_{i=1}^{N} P_i \delta(x - \xi_i)$, where $\delta(x - \xi_i)$ is the Dirac's delta function supported at $x = \xi_i$. Then, the following approximation of the solution of voltage gradient $w(x)$ is proposed in [13], [14]:

$$w(x) = \begin{cases} \dfrac{B^2}{Z^4}\left(\displaystyle\sum_{j \in \mathcal{I}_x} P_j\right)^2 (x - \xi_i) + \dfrac{G}{Z^2}\displaystyle\sum_{j \in \mathcal{I}_x} P_j & \\ +f(\xi_i), & \xi_{i+1} < x < \xi_i, \\ \dfrac{G}{Z^2}\displaystyle\sum_{j \in \mathcal{I}_{\xi_{i+1}}} P_j + f(\xi_i), & x = \xi_i - 0, \\ \dfrac{G}{Z^2}\displaystyle\sum_{j \in \mathcal{I}_{\xi_i}} P_j + f(\xi_i), & x = \xi_i + 0, \\ 0, & \xi_1 < x \leq L \end{cases} \tag{2}$$

where $Z := \sqrt{G^2 + B^2}$, $i \in \{1, \dots, N\}$, $\xi_{N+1} := 0$ and

$$f(\xi_i) = \sum_{j \in \mathcal{I}_{\xi_i}} \left\{ \left(\sum_{k \in \mathcal{I}_{\xi_{j+1}}} P_k \right)^2 \frac{B^2}{Z^4}(\xi_{j+1} - \xi_j) \right\}. \tag{3}$$

B. PROPOSED SYNTHESIS ALGORITHM

The synthesis algorithm is based on the physical insight derived with the approximate solution. By definition, the zero voltage gradient, $w(x) = 0$, implies no change of the voltage amplitude $v(x)$. We see from (2) that $w(x)$ is piecewise-affine in x, where there are multiple discontinuous points $x = \xi_i$ due to the presence of charging stations and loads. Here, we focus on the terms including $\sum_{j \in \mathcal{I}_x} P_j$ in (2) for the synthesis. It is stated in [13], [14] that the magnitude of x-dependent term in (2) is much smaller than the magnitudes of the other terms in normal setting of distribution grids. Therefore, we see that if the sum $\sum_{j \in \mathcal{I}_x} P_j$ is zero at $x \in (0, L)$, then $w(x)$ is approximately zero, that is, $v(x)$ does not change near x. Because the voltage amplitude at the starting point, $v(\xi_{N+1} = 0)$ is normally regulated within a nominal range, shaping the voltage gradient $w(x)$ in a recursive manner from the end point of the feeder can reduce the deviation of voltage amplitude $v(x)$ from the nominal. Here, we point out that the above procedure does not necessarily lead to the perfect provision of active power demanded as a PFC signal to DSO. Thus, the calculated charging/discharging power at each station is refined to achieve the perfect provision. This is conducted from the charging station closest to the bank in order. Thus, it is possible to determine the values of charging/discharging active power of each station in terms of both the voltage impact and the PFC signal. The details of the algorithm are presented in [14].

We again suppose that multiple (N_{sta}) charging stations and loads are connected to the single feeder in Figure 1. The synthesis algorithm is shown in Algorithm 1 and returns the values of charging/discharging active power for the N_{sta} stations, denoted by $P_{\mathrm{EVs},i}$ $(i = 1, \dots, N_{\mathrm{sta}})$, using the following input data:

- P_{ref}: Active power (or value of PFC signal) demanded as AS to DSO that manages the feeder and commands EVs at charging stations to charge, discharge, or stop;
- N_{sta}: Total number of the charging stations;
- $\xi_{\mathrm{sta},i} \in \{\xi_1, \dots, \xi_N\}$ $(i = 1, \dots, N_{\mathrm{sta}})$: Location of i-th charging station;
- $[\underline{P}_i, \overline{P}_i]$: Range of possible charging/discharging power by a group of EVs (in-vehicle batteries) connected to the i-th station, where $\underline{P}_i \leq 0$ for charging and $\overline{P}_i \geq 0$ for discharging;
- N_{L}: Total number of loads;
- $\xi_{\mathrm{L}j} \in \{\xi_1, \dots, \xi_N\}$ $(j = 1, \dots, N_{\mathrm{L}})$: Location of j-th load; and
- $P_{\mathrm{L}j}\,(\leq 0)$ $(j = 1, \dots, N_{\mathrm{L}})$: Power consumption of j-th load.

[1] Note that the algorithm here works for synthesizing the compensation of reactive power [14].

Algorithm 1 Determination of Charging/Discharging Active Power of In-Vehicle Batteries

$i \leftarrow 1, j \leftarrow 1, P_{\text{residual}} \leftarrow 0$
while $i \leq N_{\text{sta}}$ **do**
  if $P_{\text{residual}} \neq 0$ **then**
    $P_{\text{EVs},i} \leftarrow P_{\text{residual}}$
    $P_{\text{residual}} \leftarrow 0$
  else
    $P_{\text{EVs},i} \leftarrow 0$
  end if
  while $\xi_{\text{L}j} > \xi_{\text{sta},i}$ **do**
    $P_{\text{EVs},i} \leftarrow P_{\text{EVs},i} - P_{\text{L}j}$
    if $P_{\text{EVs},i} > \overline{P}_i$ **then**
      $P_{\text{residual}} \leftarrow P_{\text{EVs},i} - \overline{P}_i$
      $P_{\text{EVs},i} \leftarrow \overline{P}_i$
      $j \leftarrow j + 1$
      break
    else if $P_{\text{EVs},i} < \underline{P}_i$ **then**
      $P_{\text{residual}} \leftarrow P_{\text{EVs},i} - \underline{P}_i$
      $P_{\text{EVs},i} \leftarrow \underline{P}_i$
      $j \leftarrow j + 1$
      break
    end if
    $j \leftarrow j + 1$
  end while
  $P_{\text{ref}} \leftarrow P_{\text{ref}} - P_{\text{EVs},i}$
  $i \leftarrow i + 1$
end while
$i \leftarrow i - 1$
while $(P_{\text{ref}} \neq 0) \wedge (i \geq 1)$ **do**
  if $P_{\text{EVs},i} + P_{\text{ref}} > \overline{P}_i$ **then**
    $P_{\text{ref}} \leftarrow P_{\text{ref}} - \overline{P}_i + P_{\text{EVs},i}$
    $P_{\text{EVs},i} \leftarrow \overline{P}_i$
    $i \leftarrow i - 1$
  else if $P_{\text{EVs},i} + P_{\text{ref}} < \underline{P}_i$ **then**
    $P_{\text{ref}} \leftarrow P_{\text{ref}} - \underline{P}_i + P_{\text{EVs},i}$
    $P_{\text{EVs},i} \leftarrow \underline{P}_i$
    $i \leftarrow i - 1$
  else
    $P_{\text{EVs},i} \leftarrow P_{\text{EVs},i} + P_{\text{ref}}$
    $P_{\text{ref}} \leftarrow 0$
  end if
end while
return $P_{\text{EVs},i}$

Here, we have $N_{\text{sta}} + N_{\text{L}} = N$ and $\{\xi_{\text{sta},1}, \ldots, \xi_{\text{sta},N_{\text{sta}}}\} \cup \{\xi_{\text{L}1}, \ldots, \xi_{\text{L},N_{\text{L}}}\} = \{\xi_1, \ldots, \xi_N\}$, and we note that the indexes i, j of $\xi_{\text{sta},i}$ and $\xi_{\text{L}j}$ are chosen from the end point of the feeder to the starting one; that is, $\xi_{\text{sta},N_{\text{sta}}}$ and $\xi_{\text{L},N_{\text{L}}}$ are the nearest station and load to the bank along the feeder line. Since we aim the PFC reserve, P_{ref} is regarded as a part of the amount of active power required for stabilization of the grid's frequency. Several methods for determining the value of P_{ref} are reported in [8], [24].

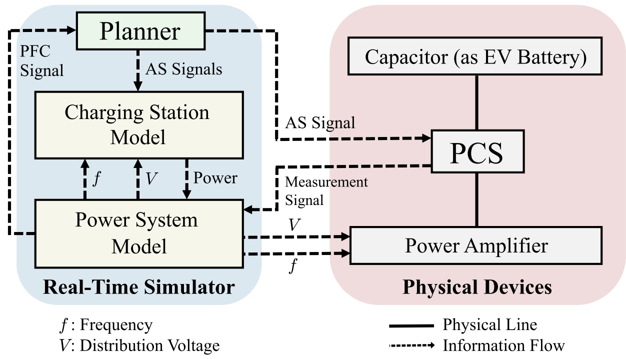

FIGURE 2. Overview of Power-HIL (Hardware-In-the-Loop) testbed which we use in this paper. The testbed includes a real-time digital simulator and physical devices coupled via power and communication lines.

III. POWER-HIL (HARDWARE-IN-THE-LOOP) TESTBED

In this section, we delineate the Power-HIL testbed for experimental validation of the Multi-Objective AS, which is a laboratory environment of a real-time digital simulator and physical devices.

A. OVERVIEW

Figure 2 shows the system overview of Power-HIL testbed for validating the Multi-Objective AS. The testbed includes a real-time digital simulator and physical devices of PCS, power amplifier, and capacitor as described in [21], [22] and below. In the real-time digital simulator, the dynamics of frequency and distribution voltage profiles are simulated with models of transmission and distribution grids, denoted by "Power System Model" in Figure 2. The regulation signal of PFC, denoted by "PFC Signal" in Figure 2, aims to regulate the balance of supply and demand in a target transmission grid. PFC signal is generated with the above-mentioned model and is sent to "Planner" as in Figure 2. Planner is the key commander of the Multi-Objective AS and generates the AS signals according to the synthesis algorithm in Section II. Namely, Planner determines the values of charging/discharging active power for all charging stations in a distribution grid, denoted by "AS Signal(s)" in Figure 2. In this sense, Planner has a function of supervisor for both distribution and transmission grids, which is partly similar to not only DSO but also a central load-frequency controller in an interconnected transmission grid. The generated "AS Signals" are sent to "Charging Station Model" on the real-time simulator. This model simulates the charging/discharging power of groups of EVs according to the AS signals. In addition to the digital simulator, the AS signal is sent via a communication line to the physical device "PCS" in Figure 2 as another group of EVs. The Power-HIL testbed is thus closed in loop by sending the signal to PCS, measuring its actual value of charging/discharging power, and receiving the measured signal at Power System Model. PCS is also connected to Power System Model through "Power Amplifier" that emulates in the physical domain the spatio-temporal change of

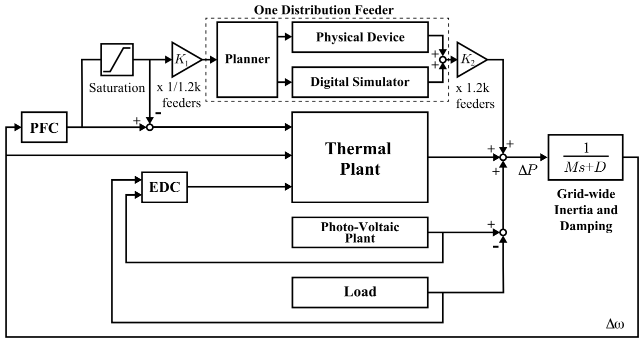

FIGURE 3. Block diagram of the frequency dynamics of transmission grid including Primary Frequency Control (PFC), Economic Dispatch Control (EDC), and distribution grid connected to electric vehicles that provide the Multi-Objective Ancillary Service (AS).

distribution voltage. This forms the other closed-loop in the Power-HIL testbed.

B. POWER SYSTEM MODEL

Next, we describe the mathematical models of transmission and distribution grids denoted by "Power System Model" in Figure 2.

A standard lumped-parameter model for the balancing of supply and demand [25] is used for simulating the frequency dynamics of a transmission grid as shown in Figure 3. The setting of the grid is based on [21], where we suppose that the transmission grid is spanned in a geographical region with a population of approximately 9 million customers. The electricity demand in the transmission grid is based on a practical dataset from Tokyo Electric Power Company, Ltd., Japan and varies in time. The grid's capacity is about 8.3 GVA, and the maximum (or minimum) demand is about 8.28 GW (or 4.8 GW). We also assume that the Photo-Voltaic (PV) generation is installed as a mega solar plant with 20% against the grid's capacity, which follows the target value in 2030 for Tokyo Electric Power Company, Ltd. One aggregated model of thermal power plant with turbine and speed governor is assumed. A function of Economic Dispatch Control (EDC) is also assumed to calculate its signal with the difference between the time-varying demand and PV generation. The details of the plant model and EDC are presented in [21]. The net imbalance ΔP of supply and demand in the grid is calculated with the output of thermal plant and the PV generation, the charging/discharging power of EVs, and the consumed power in loads including a distribution grid, as shown in the upper black of Figure 3. The deviation $\Delta\omega$ of the grid's frequency from the nominal, 50 Hz, is determined with the net imbalance ΔP, the grid-wide inertia M, and its damping coefficient D. The inertia and damping coefficient in time are 9 s and 2 s, respectively, which are the same as in [21]. PFC signal is calculated with $\Delta\omega$ and sent to the thermal plant and Planner. The scheme for the calculation is described in Figure 5 of [21] and based on the PI control with anti-windup function. The calculated PFC signal is preferentially assigned to Planner, that is, EVs in the distribution grid, and its residual is assigned to the thermal power plant.

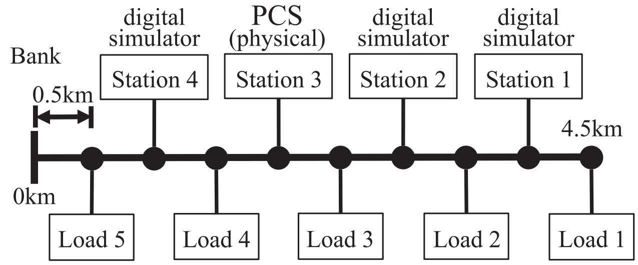

FIGURE 4. Model of one distribution feeder used for experimental validation. The third charging station "Station 3" is emulated with Power Conditioning System (PCS), and the others stations with the real-time digital simulator.

We here introduce the model of distribution grid that is included in the upper block (encompassed by the *broken* line) in Figure 2. It is assumed that 1200 same feeders of the distribution grid are connected to the transmission grid. Figure 4 shows the model of one feeder that is a single, straight-line feeder with length 4.5 km based on Figure 1 and [13], [14]. The feeder has the five loads and four charging stations located at a common interval of 0.5 km. The secondary voltage at the bank is regulated at 6.6 kV. The loading capacity of the bank transformer is set at 12 MVA, and the feeder's resistance (or reactance) at 0.227 Ω/km (or 0.401 Ω/km). The values set above are from the standard condition of medium-voltage distribution grids in Japan. All electrical components in the distribution grid are modeled with `SimPowerSystems` in MATLAB/Simulink such as voltage sources in the distribution substation, distribution lines, pole transformers, customer loads, and charging stations. The customer loads and charging stations are modeled as constant power sources. Electrical transients for inductors of lines and transformers are also considered. Their time constants are sufficiently small by comparison with those of the frequency dynamics of the transmission grid and of the inverter's response. In the following analysis, we suppose that there are 100 EVs for each charging station, where each EV has rated power output of 3 kW from [21]. That is, the maximum output power of each station corresponds to 300 kW. The loads in the distribution feeder are represented as constant power model; 600 kW for Load 1, Load 3, and Load 5, and 900 kW for Load 2 and Load 4. The maximum consumption in one feeder is set at 40% of the loading capacity of the bank. Each charging station receives the value (command) of charging/discharging power from Planner. In Figure 4, "Station 3" is built as PCS, and the other stations are built on the digital simulator. No voltage regulation device is considered in the following analysis because we simply quantify the effectiveness of the synthesis algorithm for the regulation support. Related to this, the time-varying PV generation is considered in the model of transmission grid not distribution one.

C. EXPERIMENTAL SETUP

Figure 5 is a picture of overall configuration of the Power-HIL testbed. The real-time digital simulator is manufactured by

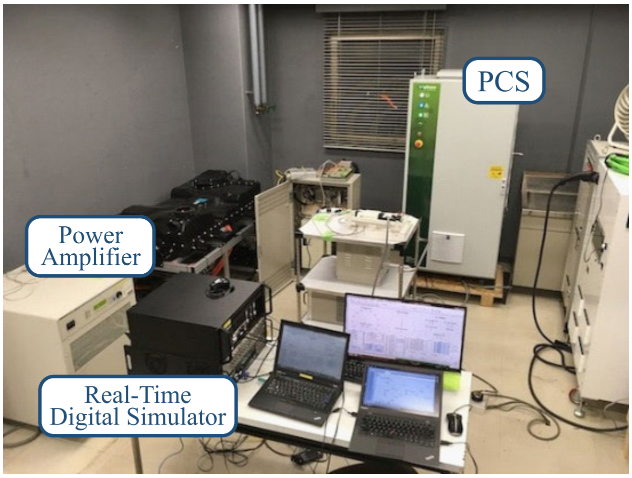

FIGURE 5. Configuration of Power-HIL (Hardware-In-the-Loop) testbed. It contains the real-time digital simulator OPAL-RT Technologies (Model #OP5600), the power amplifier AMETEK (Model #MX15-1pi), and the Power Conditioning System (PCS) Triphase NV (Model #PM15).

OPAL-RT Technologies (Model #OP5600) and located in the lower part of the figure. All the models including the distribution grid and Planner were implemented with MATLAB/Simulink, esp. `SimPowerSystems`. The time step for the digital simulation is 100 μs for calculation of the frequency deviation, the distribution voltage calculation, and the charge/discharge power for the charging stations. The setting of the time step is enough to tractable simulation of the distribution grid that exhibits the fastest transient phenomenon in the lines. PFC and AS signals are available every time step, namely 100 μs. The power amplifier is manufactured by AMETEK (Model #MX15-1pi; Rated AC output power is 15 kVA), which is located in the left part of Figure 5, and is used for the physical emulation of the frequency dynamics and the distribution voltage profile that are provided to PCS. PCS is manufactured by Triphase NV (Model #PM15; 15 kVA unidirectional power module) in the upper part of the figure and is used for the physical simulation of charging/discharging operation of the third station "Station 3." In this testbed, the transmission of signal among the digital simulator and the physical devices was Gigabit ethernet in the laboratory, therefore their communication delays were negligible in terms of the time scale of frequency dynamics of our interest.[2] Time-delays for local measurement and local controller, and time-lags of the physical devices are not negligible and will be thus evaluated in the Power-HIL testbed.

IV. RESULTS AND VALIDATION

In this section, we report experimental results on the Power-HIL testing and validation of the Multi-Objective AS by in-vehicle batteries.

[2]However, when the Multi-Objective AS is applied to a practical large-scale grid, the communication delays might affect its performance. This consideration is in our future work.

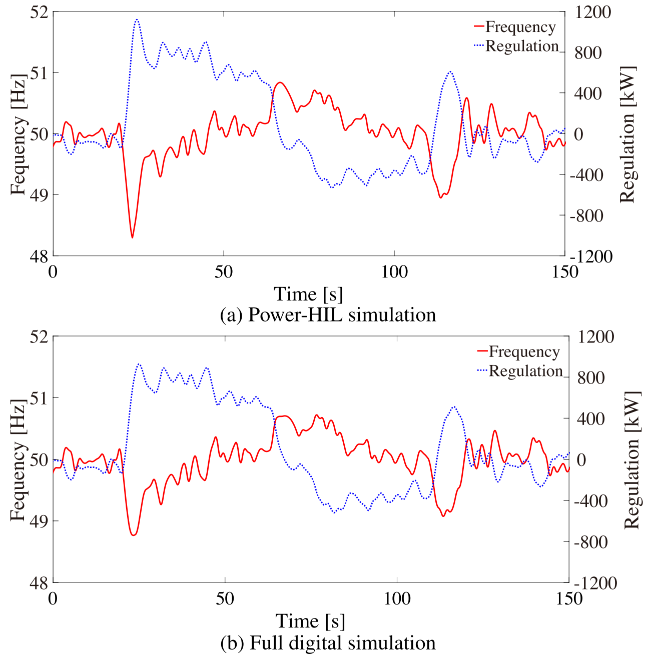

FIGURE 6. Simulation results on the AS signal to one charging station as the Primary Frequency Control (PFC) reserve and associated frequency dynamics of the transmission grid. The *blue, dotted* lines stand for the AS signals, and the *red, solid* lines for the grid's frequency.

A. PRIMARY FREQUENCY CONTROL

First, we address the provision of PFC reserve. The Power-HIL simulation of the AS signal and frequency dynamics is shown in Figure 6a. The *blue, dotted* line shows the time series of the AS signal (in power) allocated to one charging station by Planner, and the *red, solid* line does that of the grid's frequency. The positiveness (or negativeness) of the AS signals implies the discharging (or charging) operation of batteries. As introduced in Section III-B, PFC signal is calculated with the frequency deviation via the PI control. If the deviation is positive, then the signal for charging is generated; otherwise, the signal for discharging is generated. The generation mechanism is consistent with the Power-HIL simulation; for example, if the frequency is lower than the nominal (50 Hz), then the discharging operation is conducted to compensate the lack of power in the grid and thus increase the frequency. The Power-HIL result clearly shows that the frequency is regulated around the nominal.[3]

Here, we compare simulation results on the frequency dynamics and see how they are affected by the physical device. The full digital simulation of the AS signal and frequency dynamics is performed on OPAL-RT and shown in Figure 6b. The difference between the two simulations is that of model of PCS: in the full-digital simulation we use the ideal source with constant power[4]; in the Power-HIL simulation we include the real PCS. By comparison of

[3]It is noted that the frequency deviates from a standard bound in East Japan, that is, [50 Hz − 0.2 Hz, 50 Hz + 0.2 Hz]. This is mainly because the introduction rate of PV is large in the current setting, and its smoothing effect is not considered.

[4]A more detailed simulation model is discussed in [26].

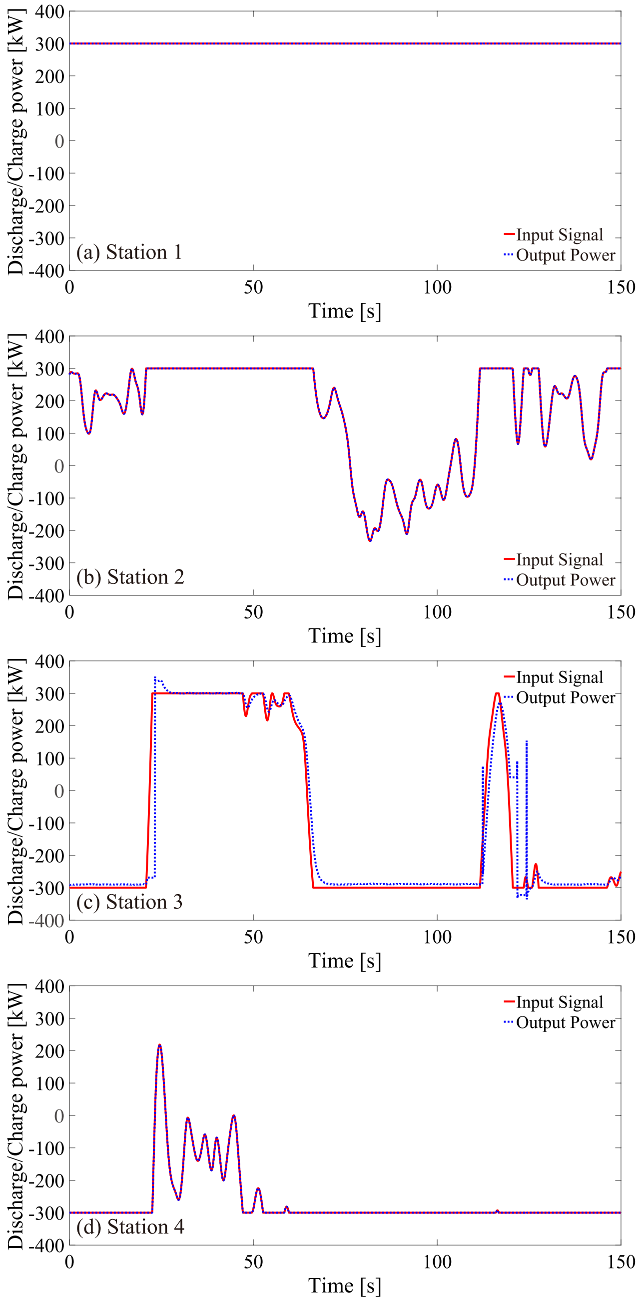

FIGURE 7. Simulation result on the input AS signals and output power of the four charging stations per a distribution feeder which are associated with Figure 6. The *red, solid* lines stand for the input signals, and the *blue, dotted* lines for the output power.

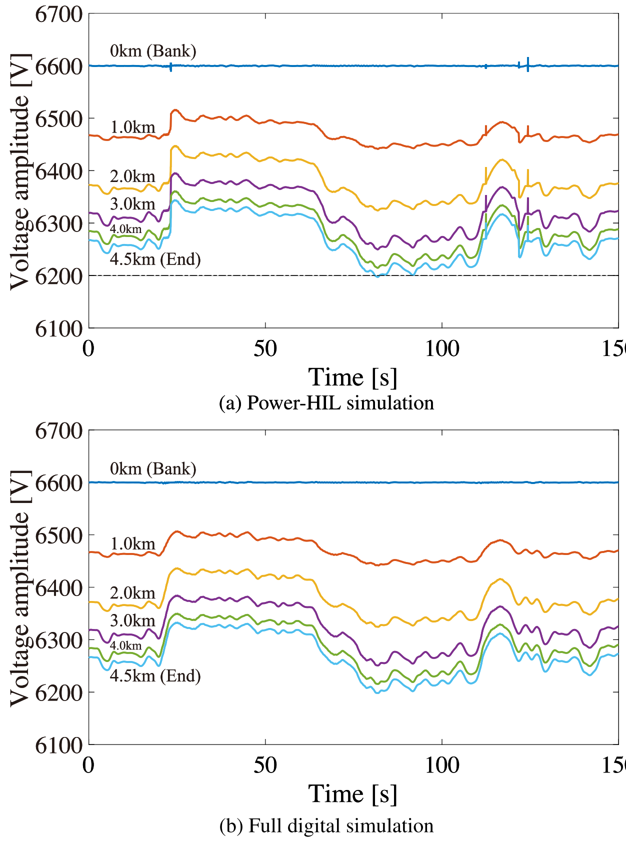

FIGURE 8. Simulation results on the distribution voltage that are associated with Figure 6. The voltages sampled at the five locations $x = 0$ km (bank), 1.0 km, 2.0 km, 3.0 km, 4.0 km, and 4.5 km (end) are plotted with different colors.

Figures 6a and 6b, we see that the magnitudes of the AS signal and frequency in the Power-HIL simulation are slightly larger than those in the full-digital simulation. For this, we show in Figure 7 the associated time series on the pairs of input AS signal and output power of the four charging stations. The *red, solid* lines in Figure 7 are the input AS signals provided by Planner, while the *blue, dotted* lines the associated output power. In the figures (a,b,d) for the three stations on the digital simulator, the time series of input signal and output power are the same because the full digital simulation does not consider any dynamics and loss of the charging/discharging operation. In the figure (c) for Station 3 as PCS, we see that the time series of input signal and output power are clearly different. More specifically, the output power of PCS shows overshoot (see the portion at about 25 s), and is delayed (see the same portion) and lagged (see at about 70 s and 110 s) with several seconds. The delay and lag are mainly due to inverter characteristics of the real PCS and measurement of the output power. They generally cause an oscillatory response and therefore the larger magnitude of output power observed in Figure 6a. Also, we see in this figure (c) impulse-like changes of the output power during [120 s, 130 s]. This is because PCS stopped to operate due to the fast fluctuation of output power, which is probably one of its design specifications.

B. DISTRIBUTION VOLTAGE SUPPORT

Figure 8a shows the distribution voltage for the Power-HIL simulation associated with Figures 6a and 7. In this figure, the voltages sampled at the five locations at $x = 0$ km (bank), 1.0 km, 2.0 km, 3.0 km, 4.0 km, and 4.5 km (end) are plotted. The voltage dynamics occur due to a combination of the AS signals to the four stations and electric (circuit) characteristics of the feeder. Also, the distribution voltage for the full digital simulation associated with Figure 6b is shown

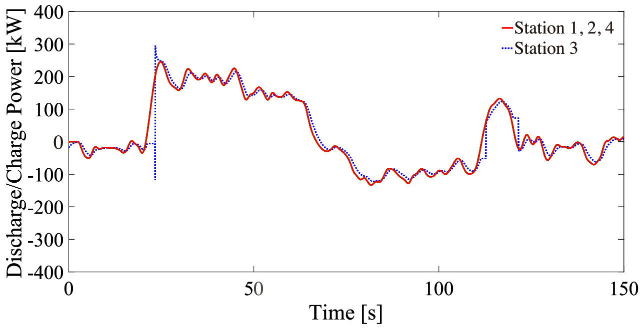

FIGURE 9. Simulation result on output power of the four charging for uniform AS signals. The *red, solid* line stands for the three stations (1,2, and 4) on the digital simulator, and the *dotted, blue* line for the third station on Power Conditioning System (PCS).

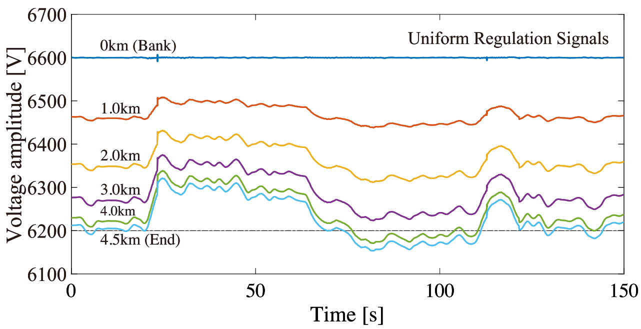

FIGURE 10. Power-HIL simulation of the distribution voltage for uniform AS signals in Figure 9. The voltage sampled at the five locations $x = 0$ km (bank), 1.0 km, 2.0 km, 3.0 km, 4.0 km, and 4.5 km (end) are plotted with different colors.

in Figure 8b. By comparison of Figures 8a and 8b, we see that the sampled changes for the Power-HIL simulation can be delayed: see, e.g., the step-wise change at about 25 s. This is mainly associated with the behavior of output power at the third station which only is built as the real PCS. Also, it is observed that impulse-like responses in the Power-HIL simulation happen according to the observation in the second paragraph of Section IV-A.

Here, we validate the synthesis algorithm in Section II, that is, generally un-equal AS signals for the four charging stations in order to mitigate the voltage impact. For this, we conduct the Power-HIL simulation in a case of uniform AS signals for the stations, where we simply divide the PFC signal by the number of the stations, i.e., 4. Figure 9 shows the time series of output power of the four stations for the uniform AS signals. In this case, the time series for the first, second, and fourth stations on the digital simulator are the same. Because the third station is built as PCS, its time response is different and affected by its physical characteristics. As discussed above, we see that the time response of the third station is impulsive (see at about 25 s) and delayed relative to that of the other stations. The Power-HIL simulation on the distribution voltage for the uniform case is shown in Figure 10. We see that the voltages at the same five locations become far from the nominal value, 6600 V, by comparison with the synthesized case in Figure 8a. This is clearly confirmed for the fourth and fifth stations; the voltages in Figure 10 decrease under the dotted line (6200 V), while the voltages in Figure 8a do not. The Power-HIL simulations show that the synthesis algorithm works effectively for the regulation support of distribution voltage.

V. CONCLUSION

This paper reported the Power-HIL testing on the Multi-Objective AS provided by in-vehicle batteries. We show that the Multi-Objective AS is consistently simulated in the physics-inclusive environment and works effectively in a dynamic situation of the grid's frequency and distribution voltage profile.

We envision several research directions. A further consideration of the AS performance, in particular, communication delay is crucial and listed up as the next testing. A refinement of the simulation model based on the Power-HIL result is also necessary, which is partly discussed in [26] for PCS. A multi-domain HIL simulation of energy system and vehicle one is challenging but could be tackled, e.g., with multi-agent simulations.

ACKNOWLEDGMENT

The authors would like to thank Mr. S. Yumiki (Osaka Prefecture University, Osaka, Japan) for his careful reading of this manuscript.

REFERENCES

[1] T. Sousa, H. Morais, Z. Vale, P. Faria, and J. Soares, "Intelligent energy resource management considering vehicle-to-grid: A simulated annealing approach," *IEEE Trans. Smart Grid*, vol. 3, no. 1, pp. 535–542, Mar. 2012.

[2] C. Wu, H. Mohsenian-Rad, and J. Huang, "Vehicle-to-aggregator interaction game," *IEEE Trans. Smart Grid*, vol. 3, no. 1, pp. 434–442, Mar. 2012.

[3] I. J. Perez-Arriaga, "The transmission of the future: The impact of distributed energy resources on the network," *IEEE Power Energy Mag.*, vol. 14, no. 4, pp. 41–53, Jul./Aug. 2016.

[4] Y. G. Rebours, D. S. Kirschen, M. Trotignon, and S. Rossignol, "A survey of frequency and voltage control ancillary services—Part I: Technical features," *IEEE Trans. Power Syst.*, vol. 22, no. 1, pp. 350–357, Feb. 2007.

[5] W. Kempton and J. Tomić, "Vehicle-to-grid power fundamentals: Calculating capacity and net revenue," *J. Power Sources*, vol. 144, no. 1, pp. 268–279, Jun. 2005.

[6] J. Tomic and W. Kempton, "Using fleets of electric-drive vehicles for grid support," *J. Power Sources*, vol. 168, pp. 459–468, Jun. 2007.

[7] M. D. Galus, S. Koch, and G. Andersson, "Provision of load frequency control by PHEVs, controllable loads, and a cogeneration unit," *IEEE Trans. Ind. Electron.*, vol. 58, no. 10, pp. 4568–4582, Oct. 2015.

[8] Y. Ota, H. Taniguchi, T. Nakajima, K. M. Liyanage, J. Baba, and A. Yokoyama, "Autonomous distributed V2G (vehicle-to-grid) satisfying scheduled charging," *IEEE Trans. Smart Grid*, vol. 3, no. 1, pp. 559–564, Mar. 2012.

[9] K. Clement-Nyns, E. Haesen, and J. Driesen, "The impact of charging plug-in hybrid electric vehicles on a residential distribution grid," *IEEE Trans. Power Syst.*, vol. 25, no. 1, pp. 371–380, Feb. 2010.

[10] K. Clement-Nyns, E. Haesen, and J. Driesen, "The impact of vehicle-to-grid on the distribution grid," *Electr. Power Syst. Res.*, vol. 81, pp. 185–192, Jan. 2011.

[11] J. A. P. Lopes, F. J. Soares, and P. M. R. Almeida, "Integration of electric vehicles in the electric power system," *Proc. IEEE*, vol. 99, no. 1, pp. 168–183, Jan. 2011.

[12] M. Falahi, H.-M. Chou, M. Ehsani, L. Xie, and K. L. Butler-Purry, "Potential power quality benefits of electric vehicles," *IEEE Trans. Sustain. Energy*, vol. 4, no. 4, pp. 1016–1023, Oct. 2013.

[13] N. Mizuta, Y. Susuki, Y. Ota, and A. Ishigame, "An ODE-based design of spatial charging/discharging patterns of in-vehicle batteries for provision of ancillary service," in *Proc. IEEE 1st Conf. Control Technol. Appl.*, Aug. 2017, pp. 193–198.
[14] N. Mizuta, Y. Susuki, Y. Ota, and A. Ishigame, "Synthesis of spatial charging/discharging patterns of in-vehicle batteries for provision of ancillary service and mitigation of voltage impact," *IEEE Syst. J.*, vol. 13, no. 3, pp. 3443–3453, Sep. 2019.
[15] M. Marinelli, S. Martinenas, K. Knezović, and P. B. Andersen, "Validating a centralized approach to primary frequency control with series-produced electric vehicles," *J. Energy Storage*, vol. 7, pp. 63–73, Aug. 2016.
[16] M. Chertkov, S. Backhaus, K. Turtisyn, V. Chernyak, and V. Lebedev, "Voltage collapse and ODE approach to power flows: Analysis of a feeder line with static disorder in consumption/production," 2011, *arXiv:1106.5003*. [Online]. Available: https://arxiv.org/abs/1106.5003
[17] X. Guillaud, M. O. Faruque, A. Teninge, A. H. Hariri, L. Vanfretti, M. Paolone, V. Dinavahi, P. Mitra, G. Lauss, C. Dufour, P. Forsyth, A. K. Srivastava, K. Strunz, T. Strasser, and A. Davoudi, "Applications of real-time simulation technologies in power and energy systems," *IEEE Power Energy Technol. Syst. J.*, vol. 2, no. 3, pp. 103–115, Sep. 2015.
[18] P. C. Kotsampopoulos, F. Lehfuss, G. F. Lauss, B. Bletterie, and N. D. Hatziargyriou, "The limitations of digital simulation and the advantages of PHIL testing in studying distributed generation provision of ancillary services," *IEEE Trans. Ind. Electron.*, vol. 62, no. 9, pp. 5502–5515, Sep. 2015.
[19] S. Martinenas, K. Knezović, and M. Marinelli, "Management of power quality issues in low voltage networks using electric vehicles: Experimental validation," *IEEE Trans. Power Del.*, vol. 32, no. 2, pp. 971–979, Apr. 2017.
[20] K. Knezović, S. Martinenas, P. B. Andersen, A. Zecchino, and M. Marinelli, "Enhancing the role of electric vehicles in the power grid: Field validation of multiple ancillary services," *IEEE Trans. Transport. Electrific.*, vol. 3, no. 1, pp. 201–209, Mar. 2017.
[21] H. Toda, Y. Ota, T. Nakajima, K. Kawabe, and A. Yokoyama, "HIL test of power system frequency control by electric vehicles," in *Proc. 1st e-Mobility Power Syst. Integr. Symp.*, 2017, p. 6.
[22] S. Kamo, Y. Ota, T. Nakajima, H. Toda, K. Kawabe, and A. Yokoyama, "HIL test on voltage management of distribution power system by smart inverter control of photovoltaic generations and electric vehicles," in *Proc. 1st e-Mobility Power Syst. Integr. Symp.*, 2017, p. 6.
[23] Y. Susuki, N. Mizuta, A. Kawashima, Y. Ota, A. Ishigame, S. Inagaki, and T. Suzuki, "A continuum approach to assessing the impact of spatio-temporal EV charging to distribution grids," in *Proc. IEEE 20th Int. Conf. Intell. Transp. Syst.*, Oct. 2017, pp. 2372–2377.
[24] T. Masuta and A. Yokoyama, "Supplementary load frequency control by use of a number of both electric vehicles and heat pump water heaters," *IEEE Trans. Smart Grid*, vol. 3, no. 3, pp. 1253–1262, Sep. 2012.
[25] G. Andersson, "Dynamics and control of electric power systems," ETH Zürich, Zürich, Switzerland, Lecture Notes 227-0528-00, 2012.
[26] S. Kamo, Y. Ota, K. Kawabe, A. Yokoyama, C. Kashiwa, and T. Nakajima, "Autonomous voltage and frequency control by smart inverters of photovoltaic generation and electric vehicle," in *Proc. 2nd e-Mobility Power Syst. Integr. Symp.*, 2018, p. 5.

NAOTO MIZUTA received the master's degree in engineering from Osaka Prefecture University, Osaka, Japan, in 2018.

He worked on the design of energy management systems integrated with car sharing systems. In 2018, he joined Meidensha Corporation, Tokyo, Japan, where he is currently involved in the research and development of power electronics products.

Mr. Mizuta is also a member of the Institute of Electrical Engineers of Japan (IEEJ). He was a recipient of the IEEJ Excellent Presentation Award, in 2018.

SHOTARO KAMO received the master's degree in engineering from Tokyo City University, Tokyo, Japan, in 2019.

He worked on the design of voltage and frequency control using smart inverters. In 2019, he joined Nisshin Electric Company, Ltd., Kyoto, Japan.

HIDEKUNI TODA received the master's degree in engineering from Tokyo City University, Tokyo, Japan, in 2019.

He worked on the hardware-in-the-loop test of power system control using electric vehicles. In 2019, he joined Japan Airlines Company, Ltd., Tokyo, Japan.

YOSHIHIKO SUSUKI (S'01–M'05) received the Ph.D. degree in electrical engineering from Kyoto University, Kyoto, Japan, in 2005.

From 2005 to 2016, he was a Faculty with the Department of Electrical Engineering, Kyoto University. In 2016, he joined the Department of Electrical and Information Systems, Osaka Prefecture University, Osaka, Japan, where he is currently an Associate Professor. From 2008 to 2010, he was a Visiting Researcher with the Department of Mechanical Engineering, University of California, Santa Barbara, under the Japan Society for the Promotion of Science, Postdoctoral Fellowship for Research Abroad. Since 2019, he has been with the Japan Science and Technology Agency, Precursory Research for Embryonic Science and Technology. His research interests include nonlinear dynamical systems, energy systems technology, and control applications. He is also an Associate Editor of the *Asian Journal of Control* and *Nonlinear Theory and Its Applications*, IEICE.

Dr. Susuki is also a member of the Society of Industrial and Applied Mathematics, American Physical Society, and the Institute of Electronics, Information and Communication Engineers, and so on.

YUTAKA OTA (M'04) received the B.S., M.S., and Ph.D. Eng. degrees from the Nagoya Institute of Technology, Nagoya, Japan, in 1998, 2000, and 2003, respectively.

He was a Project Assistant Professor with the University of Tokyo. He is currently an Associate Professor with Tokyo City University, Tokyo, Japan. His research interests include power system monitoring and control, energy storage applications, and vehicle grid integration.

Dr. Ota is also a member of the Institute of Electrical Engineers of Japan.

ATSUSHI ISHIGAME (M'93) received the Ph.D. degree in electrical engineering from Osaka Prefecture University, Osaka, Japan, in 1993.

Since 1993, he has been a Faculty with the Department of Electrical Engineering, Osaka Prefecture University, where he is currently a Professor. From 1995 to 1996, he was a Visiting Scholar with the School of Electrical Engineering, Cornell University. His research interests include power and energy systems, system optimization, and control applications.

Dr. Ishigame is also a member of the Institute of Electrical Engineers of Japan and the Institute of Electrical Installation Engineers of Japan.